

## Fragmentation of Fe<sub>2</sub>O<sub>3</sub> nanoparticles driven by a phase transition in a flame and their magnetic properties

Sangsun Yang, Ji-Hyun Yi, Soonil Son, Junggho Jang, Igor S. Altman,<sup>a)</sup> Peter V. Pikhitsa<sup>b)</sup> and Mansoo Choi<sup>c)</sup>

National CRI Center for Nano Particle Control, Institute of Advanced Machinery and Design, School of Mechanical and Aerospace Engineering, Seoul National University, Seoul 151-742, Korea

(Received 5 May 2003; accepted 15 October 2003)

The size and crystalline phase changes of Fe<sub>2</sub>O<sub>3</sub> nanoparticles formed in a H<sub>2</sub>/O<sub>2</sub> flame have been investigated. At flame temperatures below 1350 °C, the mean particle size increased monotonously with the distance from the burner edge; but in high-temperature flames above 1650 °C, it suddenly decreased from 20 to ~3 nm with the distance from the burner edge. The results of X-ray diffraction and high-resolution transmission electron microscopy showed that this sudden reduction of the size of nanoparticles was accompanied by a partial phase transformation from the metastable  $\gamma$ -Fe<sub>2</sub>O<sub>3</sub> into  $\alpha$ -Fe<sub>2</sub>O<sub>3</sub>. We suggest the structural instability due to  $\gamma$ - to  $\alpha$ -phase transformation as a mechanism for a rapid fragmentation of 20 nm particles into 3 nm ones. © 2003 American Institute of Physics. [DOI: 10.1063/1.1632534]

The formation and characterization of magnetic nanoparticles is a subject of intense research due to their potential applications as ferrofluids, magnetoresistors, gas sensors, etc. Superparamagnetism is of great interest<sup>1-3</sup> as well, being a unique aspect of magnetism in nanoparticles.<sup>4,5</sup> Reducing the size of magnetic particles and controlling their crystalline phase have greatly influenced the need for new methods of nanoparticle synthesis.<sup>6</sup> Maghemite ( $\gamma$ -Fe<sub>2</sub>O<sub>3</sub>) nanoparticles have been widely studied.<sup>7,8</sup> Among preparation methods for  $\gamma$ -Fe<sub>2</sub>O<sub>3</sub> nanoparticles, a gas-phase route using a flame has certain advantages, one of which is that it can produce very pure  $\gamma$ -Fe<sub>2</sub>O<sub>3</sub> nanoparticles continuously.<sup>9</sup>

Here, we report an anomalous evolution of the size and the crystalline phase of maghemite nanoparticles, formed by a gas-phase route within an oxy-hydrogen flame. Oxide nanoparticles generated in a flame are known to grow continuously in size.<sup>10-12</sup> However, we found that initially growing iron (III) oxide nanoparticles on reaching the size of 20 nm were abruptly transformed into ~3 nm size particles with the increasing of the distance from the burner edge  $z$ , and the size reduction was accompanied by a phase transformation.

Iron (III) acetylacetonate precursor powder was maintained at 170 °C, providing the sublimation and the resulting vapor was fed with N<sub>2</sub> through the center of a coaxial burner inside an oxy-hydrogen flame. Hydrogen and oxygen were injected through the next two concentric annuli. The flame temperature was controlled by the [H<sub>2</sub>]/[O<sub>2</sub>] ratio. Iron (III) oxide particles were collected using a localized thermophoretic sampling device<sup>13,14</sup> and with a water-cooled quartz tube.

The mean particle size increased slightly up to approximately 19 nm with the [H<sub>2</sub>]/[O<sub>2</sub>] ratio above 0.8. Beginning

with the [H<sub>2</sub>]/[O<sub>2</sub>] ratio of 0.8 (the maximum flame temperature was around 1650 °C) an unusual phenomenon was observed. Upon reaching the value of 20 nm at the flame height of  $z \approx 35$  mm, the mean particle size dramatically decreased to less than 5 nm at  $z \approx 45$  mm. Further increase of  $z$  did not significantly change the mean particle size. Transmission electron microscope (TEM) images of iron (III) oxide particles captured at different  $z$  with the [H<sub>2</sub>]/[O<sub>2</sub>] ratio of 0.8 are shown in Fig. 1. For  $z > 45$  mm, only ultrafine particles with size less than 5 nm can be observed [Fig. 1(d)].

High-resolution TEM (HRTEM) images of iron (III) oxide particles captured at different  $z$  are shown in Figs. 2(a) and 2(b). Lattice fringes corresponding to the (220) planes of the  $\gamma$ -Fe<sub>2</sub>O<sub>3</sub> cubic system are seen for the particles collected at 20 mm [Fig. 2(a)]. For the 3 nm ultrafine particles [see Fig. 2(b)], the lattice spacings of 2.70 Å as well as 2.95 Å were observed, which agreed with those of (104) planes of  $\alpha$ -Fe<sub>2</sub>O<sub>3</sub> and (220) planes of  $\gamma$ -Fe<sub>2</sub>O<sub>3</sub>, respectively. No other phase was found.

Sharp and intense x-ray diffraction (XRD) peaks shown

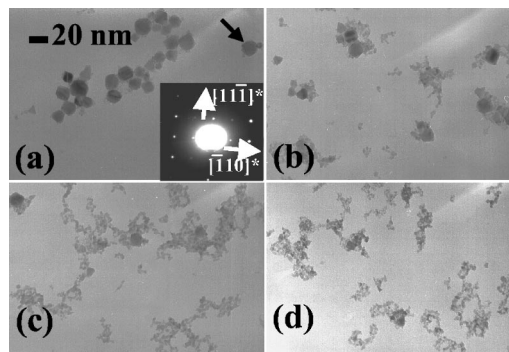


FIG. 1. TEM images of Fe<sub>2</sub>O<sub>3</sub> nanoparticles captured at (a) 35, (b) 40, (c) 43, and (d) 45 mm. The [H<sub>2</sub>]/[O<sub>2</sub>] ratio was 0.8. The selected area diffraction pattern for a 20 nm particle (indicated by the black arrow) shows that this particle is a single crystal maghemite. Particles captured at 40 mm show a distinct bimodal size distribution (the mean particle sizes of 20 nm and 3–4 nm). As  $z$  increases, the number of large particles decreases while the number of small particles increases.

<sup>a)</sup>Also at: School of Environmental Engineering, Griffith University, Brisbane 4111, Australia.

<sup>b)</sup>On leave from: Physics Institute, Odessa National University, Odessa, Ukraine.

<sup>c)</sup>Author to whom correspondence should be addressed; electronic mail: mchoi@plaza.snu.ac.kr

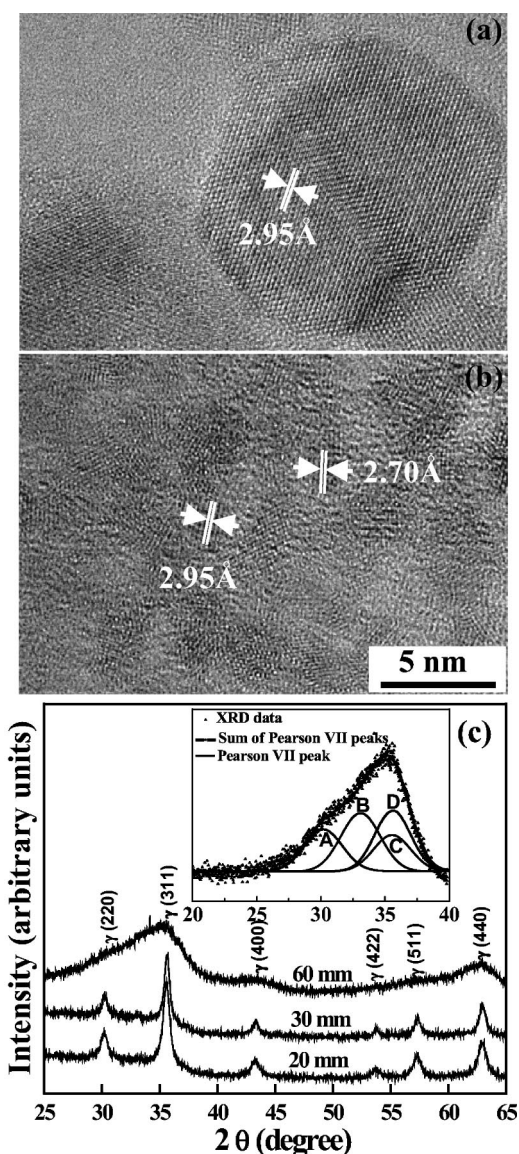


FIG. 2. Structural characterization of Fe<sub>2</sub>O<sub>3</sub> nanoparticles. (a) HRTEM image of Fe<sub>2</sub>O<sub>3</sub> nanoparticles collected at 20 mm, (b) the same at 60 mm, and (c) XRD patterns of Fe<sub>2</sub>O<sub>3</sub> nanoparticles for different *z* ([H<sub>2</sub>]/[O<sub>2</sub>]=0.8). The inset shows a fitting for the combined peak profile of the 25° to 40°(2θ) range to four Pearson VII functions for ultrafine particles.

in Fig. 2(c) prove that 20 nm particles at 20 and 30 mm were γ-Fe<sub>2</sub>O<sub>3</sub> particles. However, XRD peaks of the ultrafine particles at 60 mm were broad and weak. To resolve broad peak in the XRD pattern a fitting by Pearson VII functions<sup>15</sup> was performed. Four components were determined to ensure the required accuracy of the deconvolution [see the inset in Fig. 2(c)]. Pearson VII peaks B (2θ=33.10°) and C (2θ = 35.55°) were assigned to a (104) and a (110) reflection of α-Fe<sub>2</sub>O<sub>3</sub>, respectively. The Fe 2*p* x-ray photoelectron spectroscopy (XPS) spectrum of the ultrafine particles revealed the ion valence state of Fe (III). Since the XPS spectrum showed no Fe<sub>3</sub>O<sub>4</sub>, Pearson VII peaks A (2θ= 30.20°) and D (2θ=35.60°) should be attributed to a (220) and (311) reflection of γ-Fe<sub>2</sub>O<sub>3</sub>, respectively. The width of each of four peaks corresponds to the mean particle sizes of 2.3–2.7 nm. XRD results correspond to the conclusion made from the TEM image analysis that the sudden decrease of the particle size was accompanied by a partial phase transformation from γ- into α-Fe<sub>2</sub>O<sub>3</sub>.

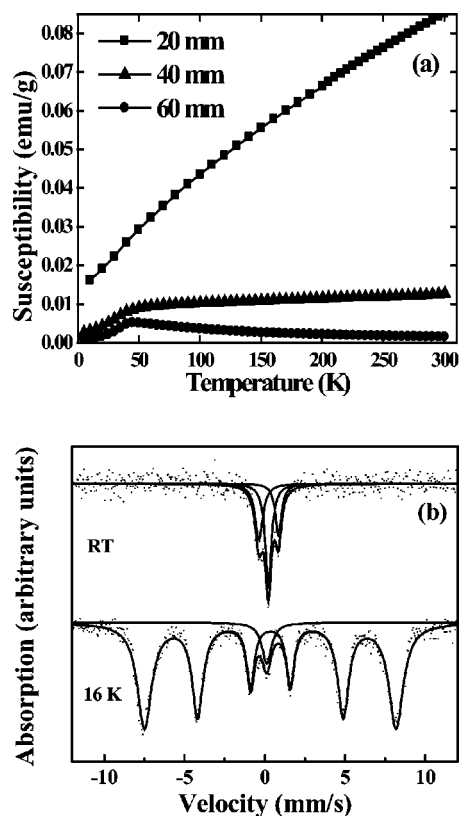


FIG. 3. Magnetic properties of Fe<sub>2</sub>O<sub>3</sub> nanoparticles. (a) Susceptibility measured at 30 G for particles collected at different *z* and (b) Mössbauer spectra of ultrafine particles at RT and at 16 K. The solid lines are the least-square fits to the experimental data.

The magnetic susceptibility of nanoparticles, measured with a superconducting quantum interference device (SQUID) magnetometer, is shown in Fig. 3(a). Markedly different susceptibilities are obtained for particles captured from the same flame, but at different heights. Note a typical superparamagnetic behavior above the blocking temperature of 45 K for ultrafine nanoparticles collected at 60 mm, which indicates a transition from ferrimagnetism to superparamagnetism. Figure 3(b) shows the Mössbauer spectra for ultrafine particles. The disappearance of the 16 K sextet (originating from the internal magnetic field<sup>16</sup>) and the appearance of the doublet at room temperature, confirms the superparamagnetic behavior concluded from the SQUID. There is also seen the singlet, which was not observed for γ-Fe<sub>2</sub>O<sub>3</sub> nanoparticles of 3 nm coated with silica.<sup>17</sup> Since the singlet line could also appear when ferric ion is in an ideal cubic environment,<sup>16</sup> the appearance of the singlet along with the doublet in our case can be interpreted as an additional ferric ion singlet, giving the reasonable parameters of the doublet with the splitting of 1.1 mm/s (to be compared with the previously reported values of 0.9 mm/s<sup>17</sup> and 1.19 mm/s<sup>18</sup>) and the isomer shift of about 0.25 mm/s for both the doublet and the singlet.

It is well known that the maghemite phase is metastable in the bulk though its stability can considerably improve in nanoscale.<sup>19</sup> At a sufficiently high temperature *T<sub>g</sub>* the energy barrier Δ ≈ 270 kJ/mol,<sup>20</sup> separating γ- and α-phases can be overcome within the short residence time of a nanoparticle in flame (about 1 ms) as far as the rate of the transformation is thermally activated.<sup>20,21</sup> The heat release due to the enthalpy

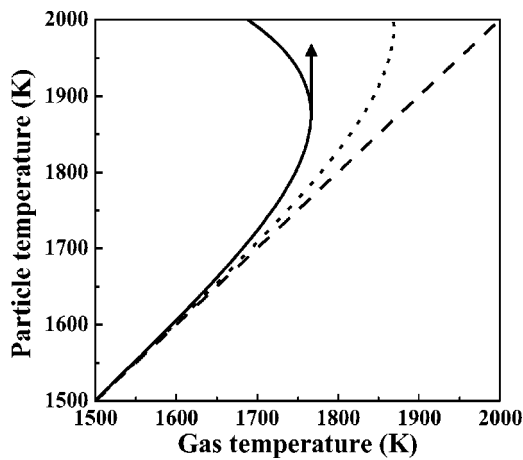


FIG. 4. The diagram of the particle temperature stability according to Eq. (1). The vertical arrow indicates the location of losing stability and the onset of the fragmentation for 20 nm particles. The dot line corresponds to 4 nm particles. The dashed line is the gas temperature shown for comparison.

difference.<sup>22</sup>  $H_{tr} = 15$  kJ/mol, between  $\gamma$ - and  $\alpha$ -phases during the fast transformation heats up the maghemite nanoparticle, which leads to the further acceleration of the increase in its temperature  $T_p$ . This feedback results in instability of the initial phase, leading to the explosive fragmentation of the maghemite nanoparticle into much smaller components, part of which has been converted into the  $\alpha$ -phase.

To locate this structural instability we use the heat balance equation that determines the particle temperature:

$$Q_{\text{heat}} - Q_{\text{cool}} = 0, \quad (1)$$

where the heat gain from the phase transformation in a particle of the radius  $r = 10$  nm, and the mass density  $\rho \sim 5$  g/cm<sup>3</sup> can be written as

$$Q_{\text{heat}} = H_{tr} \frac{4\pi r^3}{3} \frac{\rho N_A}{\mu} \frac{1}{\tau}, \quad \tau = \tau_0 \exp(\Delta/T_p), \quad (2)$$

The heat loss due to the cooling by the surrounding gas of the temperature  $T_g$  is<sup>23</sup>

$$Q_{\text{cool}} = \frac{1}{2} \frac{\gamma+1}{\gamma-1} \frac{\alpha P_g k_B (T_p - T_g)}{\sqrt{2\pi(\mu_g/N_A)k_B T_g}} 4\pi r^2. \quad (3)$$

In Eqs. (2) and (3), the molar weight is  $\mu = 160$  g/mol for the iron oxide and  $\mu_g = 29$  g/mol for air,  $N_A$  is the Avogadro number,  $\gamma = 1.4$  is the Poisson ratio for air,  $k_B$  is the Boltzmann constant,  $P_g$  is the atmosphere pressure,  $\alpha$  is the energy accommodation coefficient,<sup>23</sup>  $\tau$  is the characteristic time of the phase transition, and  $\tau_0$  is the characteristic attempt time (about  $10^{-12}$  s in our case). For simplicity, we neglected any other contributions affecting heat balance, which do not alter the results significantly.

Figure 4 provides a principal scenario (calculated with  $\alpha = 0.01$ ) for the critical behavior of the particle temperature according to Eq. (1). Note that there is evidence<sup>24</sup> that  $\alpha$  can

be very small at high temperatures. One can see that for the flame temperature exceeding 1750 K, there are no appropriate particle temperatures for the system to be stable at a given particle radius of 10 nm while they still exist for the smaller particle radius of 2 nm. Thus, on approaching the critical temperature, the particle should experience a sudden transition into some other stable state, which can be followed by the abrupt reduction of the characteristic particle size through the particle fragmentation. Since the fast high-temperature transformation towards the  $\alpha$ -phase produces mechanical strains, the natural way for the particle to keep the heat balance is to be fragmented into considerably smaller particles. Such an explosion-like (or maybe peeling-like) transformation cannot be complete, and we observe the mixture of both  $\gamma$ - and  $\alpha$ -phases in ultrafine nanoparticles of 3 nm. This fragmentation phenomenon can be used to obtain substantially different sizes and phases of nanoparticles having different properties from the same flame. We believe that the fragmentation phenomenon revealed is general and applicable for other complex oxides.

The authors gratefully appreciate C. S. Kim at Kookmin University for giving them a possibility to measure the Mössbauer spectra. SQUID measurements were done at Korea Basic Science Institute. This work was funded by the Creative Research Initiatives Program supported by the Ministry of Science and Technology, Korea.

<sup>1</sup>S. Mørup and E. Tronc, Phys. Rev. Lett. **72**, 3278 (1994).

<sup>2</sup>R. D. McMichael, R. D. Shull, L. J. Swartzendruber, and L. H. Bennett, J. Magn. Magn. Mater. **111**, 29 (1992).

<sup>3</sup>U. Häfeli, W. Schütt, J. Teller, and M. Zborowski, *Scientific and Clinical Applications of Magnetic Carriers* (Plenum, New York, 1997).

<sup>4</sup>D. D. Awschalom and D. P. DiVincenzo, Phys. Today **48**, 43 (1995).

<sup>5</sup>S. V. Vonsovskii, *Magnetism* (Wiley, New York, 1974), Vol. 2, p. 938.

<sup>6</sup>B. Martinez, A. Roig, and E. Molins, J. Appl. Phys. **83**, 3256 (1998).

<sup>7</sup>S. Y. Lin, J. Ferg, P. Biswas, R. Enzweiler, and P. Boolchand, J. Magn. Magn. Mater. **159**, 147 (1996).

<sup>8</sup>Q. Chen and Z. J. Zhang, Appl. Phys. Lett. **73**, 3156 (1998).

<sup>9</sup>M. R. Zachariah and S. Huzarewicz, J. Mater. Res. **6**, 264 (1991).

<sup>10</sup>C. Janzen and P. Roth, Combust. Flame **125**, 1150 (2001).

<sup>11</sup>D. Lee, S. Yang, and M. Choi, Appl. Phys. Lett. **79**, 2459 (2001).

<sup>12</sup>D. Lee and M. Choi, J. Aerosol Sci. **33**, 1 (2002).

<sup>13</sup>J. Cho and M. Choi, J. Aerosol Sci. **31**, 1077 (2000).

<sup>14</sup>D. Lee and M. Choi, J. Aerosol Sci. **31**, 1145 (2000).

<sup>15</sup>M. M. Hall, V. G. Veeraraghavan, H. Rubin, and P. G. Winchell, J. Appl. Phys. **10**, 66 (1977).

<sup>16</sup>N. N. Greenwood and T. C. Gibb, *Mössbauer Spectroscopy* (Chapman and Hall, London, 1971), p. 250.

<sup>17</sup>L. Zhang, G. C. Papaefthymiou, and J. Y. Ying, J. Appl. Phys. **81**, 6892 (1997).

<sup>18</sup>X. N. Xu, Y. Wolfus, A. Shaulov, Y. Yeshurun, I. Felner, I. Nowik, Yu. Koltypin, and A. Gedanken, J. Appl. Phys. **91**, 4611 (2002).

<sup>19</sup>X. Ye, D. Lin, Z. Jiao, and L. Zhang, J. Phys. D **31**, 2739 (1998).

<sup>20</sup>G. Schimanke and M. Martin, Solid State Ionics **136–137**, 1235 (2000).

<sup>21</sup>C. B. de Boer and M. J. Dekkers, Geophys. J. Int. **144**, 481 (2001).

<sup>22</sup>Ch. Laberty and A. Navrotsky, Geochim. Cosmochim. Acta **62**, 2905 (1998).

<sup>23</sup>F. O. Goodman and H. Y. Wachman, *Dynamics of Gas-Surface Scattering* (Academic, New York, 1976) p. 260.

<sup>24</sup>I. S. Altman, D. Lee, J. Song, and M. Choi, Phys. Rev. E **64**, 052202 (2001).